



HHS Public Access

Author manuscript

Curr Opin Biomed Eng. Author manuscript; available in PMC 2023 March 01.

Published in final edited form as:

Curr Opin Biomed Eng. 2023 March ; 25: . doi:10.1016/j.cobme.2022.100433.

Label-free optical imaging of cell function and collagen structure for cell-based therapies

Linghao Hu,

Samantha Morganti,

Uyen Nguyen,

Oscar R. Benavides,

Alex J. Walsh

Department of Biomedical Engineering, Texas A&M University, TX, USA

Abstract

Cell-based therapies harness functional cells or tissues to mediate healing and treat disease. Assessment of cellular therapeutics requires methods that are non-destructive to ensure therapies remain viable and uncontaminated for use in patients. Optical imaging of endogenous collagen, by second-harmonic generation, and the metabolic coenzymes NADH and FAD, by autofluorescence microscopy, provides tissue structure and cellular information. Here, we review applications of label-free nonlinear optical imaging of cellular metabolism and collagen second-harmonic generation for assessing cell-based therapies. Additionally, we discuss the potential of label-free imaging for quality control of cell-based therapies, as well as the current limitations and potential future directions of label-free imaging technologies.

Keywords

Cytherapy; Microscopy; Fluorescence; Regenerative engineering; Metabolism; Collagen

Introduction

Cell-based therapies, or cytotherapies, use either a patient's own cells or cells from a donor to mediate wound healing and combat disease. Cytotherapies often consist of immune cells, for directing immune responses, or stem cells, for tissue regeneration, and are currently in development for a range of diseases and pathologies including autoimmune disease, cancer, and wound healing [1,2]. Cell-based therapies either use a patient's own cells for an autologous transplant, or a donor's cells, which is an allogenic transplant. Often, the cells used for cytotherapies are enhanced chemically, genetically, or mechanically during the biomanufacturing process. Cytotherapies include cell-suspensions that are injected into

This is an open access article under the CC BY-NC-ND license (<http://creativecommons.org/licenses/by-nc-nd/4.0/>).

Corresponding author: Walsh, Alex J. (walshaj@tamu.edu).

Declaration of competing interest

The authors declare the following financial interests/personal relationships which may be considered as potential competing interests: Alex J Walsh has patent #11376593 issued to WARF. Alex J Walsh has patent #20210049346 issued to WARF.

patients, such as blood transfusions or chimeric antigen receptor (CAR) T cell therapies for lymphoma [3]. Alternatively, cells can be seeded on biomaterials to create biomimetic tissues which are implanted to enhance tissue regeneration [4,5].

Cell-based therapies have a common need for quality control and assessment of the living cells and biomaterials during the biomanufacturing process, since the products will be used as transplants and medicine. Many factors, from the materials and reagents to the equipment and protocols, in the manufacturing process are regulated through Good Manufacturing Practice (GMP) regulations. However, cell-based therapies often have unique starting materials and a high-level of variability that arises from the biological and living nature of cells. It is important to not only ensure safety of the cytotherapies, but also assess the efficacy of the final product [6,7]. Quality control assessments can be performed in-, on-, or off-line during the manufacturing process. In- and on-line systems can be incorporated to enable real-time or near real-time measurements and continuous monitoring of a manufacturing process. For example, in situ microscopy, which is based on back-scattered or reflected light, has been investigated for decades as an in-line optical imaging method to quantitatively assess cell concentrations within bioreactor cultures for various bioprocess such as the fermentation of yeasts or the expansion of mesenchymal stem cells on microspheres [8,9]. Traditional biochemical assays to characterize cell viability and functions, such as histology, western blot analysis, flow cytometry, and genetic sequencing or mRNA analysis, require tissue dissociation and cell fixation and therefore can only be performed off-line. While these assays are useful for characterization of cells and biomaterials during development, they are unable to be used for in- or on-line quality control of cytotherapies. Label-free optical imaging is an attractive modality for the assessment of cell-based therapies and regenerative devices because it relies on endogenous contrast and uses non-destructive light (Figure 1). Therefore, the alterations within the cells are detected by imaging without labeling, and provide a parallel reference for quality control and assurance.

Although label-free optical imaging is limited to the detection of endogenous chromophores, several endogenous molecules exhibit fluorescence including collagen, melanin, tryptophan, reduced nicotinamide dinucleotide (NADH), and flavin adenine dinucleotide (FAD) [10]. NADH and FAD are two coenzymes of metabolic reactions (Figure 2). Thus, autofluorescence imaging of NADH and FAD allows label-free detection of cellular metabolism [11,12]. NADH and FAD autofluorescence can be separated by different excitation and emission wavelengths [13]. NADH and NADPH are indistinguishable by fluorescence imaging and thus NAD(P)H is commonly used for the combined, detected signal [13]. NAD(P)H is typically excited around 370 nm for single photon fluorescence and 750 nm for two-photon fluorescence. FAD is typically excited around 405 nm for single photon fluorescence and ~890–900 nm for two-photon excitation. NAD(P)H emits fluorescence around 400–500 nm, and FAD emits around 500–600 nm [13].

The fluorescence intensity is proportional to fluorophore concentration while the fluorescence lifetime is altered due to microenvironmental changes, such as binding state for NADH and FAD [14]. Fluorescence lifetime is the time that the fluorophore is in the excited state which normally ranges from picoseconds to nano-seconds in duration

[15]. The fluorescence lifetime of NAD(P)H and FAD allows quantification of the enzyme-binding fractions of NAD(P)H and FAD, as well as the lifetimes of the free- and bound-fractions, due to binding-dependent conformational changes of NAD(P)H and FAD that alter the quenching of the fluorophore [16,17]. The fluorescence intensities and lifetimes of NAD(P)H and FAD provide quantitative metrics of cellular metabolism and have been used to distinguish neoplasia from normal tissue, identify anti-cancer drug response, and classify immune cell phenotype [18-20]. NAD(P)H and FAD fluorescence intensity can be imaged on any fluorescence microscope using the appropriate filters for excitation and emission, and fluorescence lifetime imaging of NADH and FAD is often realized on multiphoton fluorescence microscopes adapted with time-counting electronics [21].

Collagen comprises the dominant protein of the extracellular matrix, and collagen density, alignment, and tortuosity provide information about the tissue environment. The repetitive non-centrosymmetric structures of collagen fibers produce a second-harmonic generation (SHG) signal and allow a label-free visualization of fibrillar collagen (Figure 1). SHG is a nonlinear optical process in which photons interacting with a nonlinear material are combined to form new photons having twice the energy (one-half the wavelength) of the incident photons [22,23]. SHG microscopy uses the same microscope hardware and illumination laser as multiphoton fluorescence imaging and has similar resolution and light penetration depths. SHG microscopy can be performed on thick tissues or biomaterials *in vivo* and *in vitro* [22]. The SHG images of collagen fibers can be processed by multiple approaches such as Fourier transform, texture analysis, and individual fiber segmentation to obtain morphological features [22]. SHG imaging is useful for imaging the ECM of tissues and biomanufactured tissue scaffolds as collagen is a major component of the ECM.

Label-free optical imaging provides advantages over other optical imaging techniques for quality control of cytotherapies. Although collagen architecture can be detected by other imaging techniques, such as polarized light microscopy (PLM) [24], optical coherence tomography (OCT) [25], and Raman spectroscopy [26-28], SHG imaging provides high specificity for collagen detection and high spatial resolution at depths up to ~ 1 mm in tissue [29]. Similarly, NADH, FAD, and collagen structures can also be imaged with single-photon excitation, but the red-shifted excitation light of nonlinear imaging techniques including SHG imaging and autofluorescence lifetime imaging enables increased light penetration in 3D samples and tissues. The longer wavelengths of light and optical sectioning properties of multiphoton excitation also reduce photobleaching. While collagen fluorescence can be imaged by either single- or multi-photon excitation by light-sheet scattering microscopy [30], and confocal microscopy [31,32], the fluorescence emission of collagen overlaps with other tissue chromophores including NAD(P)H, flavins, elastin, and lipofuscin. Therefore, SHG imaging provides better visualization of fibrillar collagen architecture than autofluorescence imaging. Furthermore, fluorescence lifetime imaging is independent of factors that influence intensity imaging such as light scattering, laser power, and fluorophore concentration, and provides information regarding the molecule structure, and surrounding microenvironments [33].

Autofluorescence imaging for quality control of cytotherapies

Autofluorescence imaging of immune cells may provide a label-free and non-contact method to assess cytotherapies during the manufacturing process (Figure 3). Many cytotherapy approaches harness the innate abilities of immune cells to combat disease, due to the diverse functions of immune cells which can be optimized through genetic and chemical manipulation. For example, in CAR T cell therapies, an FDA-approved cytotherapy, T cells are removed from the blood of a cancer patient, the T cells are genetically engineered to express the anti-cancer receptor CAR and activated, and then the T cells are injected into the patient. Since cytotherapies inject cells directly into patients, a number of quality control and quality assurance standards must be met in the manufacturing process. Assessments of the cell therapies must either be non-contact and non-damaging or performed on a parallel sample of cells so that the sterility and function of the cells is not compromised. Optical imaging which is non-destructive and non-contact may fill a critical role for in-line quality control of cell therapies.

Immune cell function, particularly for T cells and macrophages, is dependent on metabolic switches between glycolysis and oxidative phosphorylation [34,35]. NADH and FAD fluorescence lifetime imaging of T cells, combined with machine learning for cell classification, revealed autofluorescence lifetime differences between quiescent and activated T cells and achieved >99% accuracy for identification of T cell state from the autofluorescence lifetime features [36]. Classification of T cell states of quiescence or activation is also possible from NAD(P)H intensity images [37], suggesting that imaging flow cytometers may be adapted for quality control assessment and sorting of T cell therapies. Currently, autofluorescence imaging has not been implemented into the quality assurance and quality control manufacturing practices for cytotherapy processes. However, NAD(P)H and FAD imaging provides a unique metric of cellular metabolism and function that may help optimize cytotherapies, such as CAR T cell therapies, by non-invasively evaluating cellular status and sorting cells by phenotype before injecting the cells into patients (Figure 3).

Similarly, autofluorescence intensity and lifetime imaging of NAD(P)H and FAD allow identification of macrophage polarization [36,38,39]. There are two well-classified macrophage phenotypes, classically activated, pro-inflammatory macrophages (“M1-like”) and alternatively activated, pro-healing (“M2-like”) macrophages [34]. While M2-like macrophages promote cancer proliferation and suppress the attack from immune cells, M1-like macrophages exhibit antitumor activities including apoptotic or phagocytic signaling, secondary immune stimulation, and nutrient deprivation of tumor cells [15]. M1-like macrophages and M2-like macrophages use different metabolic pathways to generate energy [40]. M1-like macrophages have upregulated glycolysis while M2-like macrophages generally are more dependent on oxidative metabolism [34]. These metabolic differences between M1-like and M2-like macrophages are detected by autofluorescence imaging of NAD(P)H and FAD [41-45]. High resolution optical imaging, combined with single-cell segmentation, allows quantification of the changes in metabolism at the cell level, and successfully distinguishes subpopulations of macrophages [15]. Macrophage cell-based therapies are being developed for hereditary pulmonary alveolar proteinosis [46], and

autofluorescence imaging of macrophages for quality control pre-injection may improve these cell-based therapies. Additionally, macrophages mediate stem-cell interactions and the wound healing process, and thus are important to characterize in preclinical studies of regenerative cytotераpy devices.

Autofluorescence imaging of stem cells for tissue regeneration

Stem cells have potential for use in regenerative medicine devices since stem cells can self-replicate and have the potential to develop into many different types of cells. Cardiomyocytes (CMs) are cells that build up the muscles in and around the heart. These cells are terminally differentiated with no regenerative capacity [47]. Studies have established a variety of methods to generate CMs from human pluripotent stem cells (hPSCs), however, batch -to-batch and line-to-line variability in the differentiation process reduces the efficiency of CM manufacturing [47]. Autofluorescence lifetime imaging of CM during differentiation identified differences between differentiation outcomes that could be predicted from the imaging features as early as day 1 [47]. Using a logistic regression-based classifier and 13 autofluorescence intensity and lifetime variables, the model predicted high and low differentiation efficiencies with an accuracy over 85%, and the model performance was 0.91 (AUC of ROC) [47].

Glioma stem cells (GSCs) are believed to be responsible for tumor formation, progression, treatment resistance, and recurrence [48]. The identification and isolation of GSCs are crucial for research in GSC-targeting therapies. Past studies have shown NAD(P)H fluorescence intensity and fluorescence lifetime of bound and free NAD(P)H have been used to distinguish stem cells from their differentiated offspring [48]. A recent study has found that it is possible to sort cells using fluorescence-activated cell sorting (FACS) based on the autofluorescence intensity of NAD(P)H [48]. The glioma cells within the top 10% of NAD(P)H intensity are labeled as NADH^{high}. These cells were shown to exhibit the same characteristics of GSCs *in vitro*, as well as having high tumorigenicity *in vivo* [48]. The study also showed the intensity of NAD(P)H autofluorescence can be used as a biomarker to isolate cancer stem cells (CSCs) in breast cancer and colon cancer, proposing this biomarker might be an extensive biomarker for CSCs [48].

Understanding the metabolic basis of the CSC phenotype is crucial in research of new drug therapies that could reduce tumor recurrence and metastasis. A recent study has indicated high NAD(P)H autofluorescence levels and increased mitochondrial oxidative stress are both key characteristics of the CSC metabolic phenotype [49]. This was determined by studying the phenotype of cells with high levels of NAD(P)H autofluorescence. CSCs may depend on NAD(P)H to maintain their enhanced mitochondrial function as high levels of NAD(P)H autofluorescence is known to be a marker for mitochondrial metabolism, high OXPHOS capacity, and increased ATP production [49]. Autofluorescence imaging of stem cells has the potential for future use in the evaluation of stem-cell based therapies, for the testing of drugs to direct stem cell differentiation, and for the determination of stem cell roles in the development of various diseases.

Imaging collagen to track tissue regeneration

The visualization of fibrillar collagen via SHG imaging allows quantification of collagen fibers during tissue regeneration and in response to therapy. SHG imaging was used to assess collagen continuity throughout the recovery progress in nerves that were subjected to low strain and high strain injuries [50]. From the SHG images of endoneurial collagen, full nerve regeneration was observed in the low strain nerves, while evidence of partial regeneration was found in high strain nerves [50]. Furthermore, recent studies have used SHG imaging to identify temporal and spatial changes in extracellular matrix (ECM) remodeling, regeneration, and recapitulation in wounded corneas [51,52]. As wound healing progresses, the collagen in fibrotic tissue is dramatically remodeled into a normal, interwoven pattern with an orthogonal arrangement, and maintains transparency and thickness [51,52]. To characterize the wound healing process, SHG microscopy was used to quantitate collagen after nerve repair, and collagen fibers were found to be more aligned in the control nerves than in the damaged nerves [53]. A combination of SHG imaging with tissue clearing allows assessment of cardiac fibrosis necrosis and regeneration in Duchenne muscular dystrophy [54]. Due to the association between collagen fiber alignment and stage of tissue regeneration, SHG imaging to visualize collagen fibers allows a label-free imaging modality to quantitatively analyze fibrillar collagen for assessing tissue regeneration.

A variety of collagen-based scaffolds have been fabricated and used to support cells for in-vitro tissue models. The properties of the engineered scaffolds are similar to the ECM, and their structure and composition modify cellular activities *in vitro* or *in vivo*. Although the SHG intensity of collagen fibers grown *in vitro* is an order of magnitude lower than that of native collagen fibers [55], SHG imaging of collagen scaffolds allows characterization of collagen fibers and study of cell–matrix interactions without staining (Figure 4). For example, SHG imaging was used to quantify the spatial organization of synthesized collagen scaffold fibers under dynamic conditions [56]. Additionally, SHG imaging was used to characterize collagen structure and strain state alterations of porous collagen-GAG scaffolds seeded with human umbilical vein endothelial cells (HUVECs), and human mesenchymal stem cells (hMSCs) over 10 days [57]. Compared to the control scaffolds without cells, collagen reorganization and vessel-like architecture formation were found in the cell-seeded collagen scaffolds [57]. Furthermore, the collagenous scar in porous collagen-based scaffolds (PCSs) was visualized with SHG imaging to study the effects of neural stem cell (NSC) grafts on spinal cord injury recovery [58]. The NSC-seeded PCS grafts promoted neuronal differentiation and locomotion to induce regeneration [58]. SHG imaging has also been used to reveal the collagen structure in decellularized tissues to investigate metastatic nests of cancer cells [59].

Multimodal autofluorescence and SHG imaging for tissue regeneration

Because SHG and autofluorescence microscopy require similar hardware, collagen SHG signals and autofluorescence can be simultaneously imaged with multiple spectral channels. The optical redox ratio (NAD(P) H/FAD) and quantitative parameters of collagen content via SHG imaging have been tracked in breast cancer progression and recession throughout chemotherapy treatments [61]. A higher optical redox ratio was observed in the tissue with

carcinoma compared to the healthy tissues indicating a high metabolic rate, and the optical redox ratio decreased during chemotherapy [61]. Collagen density, quantified from SHG images, revealed that the collagen degenerates with tumor progression and regenerates post-chemotherapy [61]. Likewise, autofluorescence imaging combined with SHG imaging, has been used to evaluate engineered skeletal muscle units (SMU) before implantation [62]. The optical redox ratio was found to differentiate the control from the experimental group that was metabolically stressed due to reduced feeding frequency, while the SHG signal from myosin and collagen was used to distinguish control SMUs from the steroid supplemented group [62]. NAD(P)H fluorescence lifetime of tumor cells and SHG imaging of collagen within tumors has been used to evaluate tumor response to chemotherapy in a mouse model of colorectal cancer [63].

Although the combination of autofluorescence lifetime imaging with SHG imaging is currently underexplored for the characterization of cell-seeded biomaterials and scaffolds, we expect increased use of autofluorescence lifetime imaging concurrent with SHG imaging for characterization of regenerative engineered devices. NAD(P)H and FAD fluorescence lifetime imaging allows differentiation of macrophage phenotypes, due to their different metabolic activities [41-45]. Since the pro-inflammatory macrophage (M1) and anti-inflammatory macrophage (M2) macrophages exhibit different immune functions, autofluorescence imaging can be used to study macrophage polarization states to monitor wound healing progression. Autofluorescence imaging combined with SHG imaging has been used to study macrophage metabolism and collagen structure for macrophages seeded on extracellular matrices with either random or aligned fiber configurations [64]. In a one-week trial, the preliminary results reveal significant changes in fluorescence lifetime features with time, and between anisotropic and isotropic ECM [64].

Cytherapy transplants autologous or allogeneic cellular materials to replace or repair damaged tissues and cells. The general procedure involves cell isolation, genetic engineering, injection, and infusion. Therefore, characterization of cellular viability and phenotype is necessary to ensure the effectiveness and safety of therapy before reintroduction to the patients. Label-free optical imaging techniques allow a non-destructive visualization and quantification of cell phenotypes and collagen structures within the ECM.

Time-domain fluorescence lifetime measurements are commonly performed with pulsed excitation and time-correlated single photon counting (TCSPC). Despite the advantages of label-free nonlinear imaging techniques for assessing cellular phenotypes and tracking tissue regeneration, technical challenges remain to be addressed for quality control and assurance applications for cytherapy manufacturing, and for *in vivo* monitoring of tissue regeneration. Multiphoton imaging systems need to be adapted for in-line assessments of manufactured cells or tissues. Fluorescence lifetime imaging requires a pulsed excitation source and specialized detectors. In addition, the acquisition time of lifetime imaging is longer compared to intensity imaging, since more photons are needed to accurately fit the decay curve, and the data analysis also requires specific expertise and is time-consuming. Recently, several fluorescence lifetime cytometers have been developed to achieve cell sorting and counting based on lifetime measurements [65-67]. However, current fluorescence lifetime cytometers measure a single average lifetime of each cell instead of

obtaining multi-exponential decay information. To address this limitation, several studies have improved imaging speed by using high-performance time-correlated single photon counting (TCSPC) and optimized scan methods [68,69]. Furthermore, fast lifetime imaging, realized with pulsed single-photon excitation and a time-tagger device, of T cells can detect activation, demonstrated feasibility for integration of fluorescence lifetime imaging into flow cytometry for quality control in cytotherapy [70]. Alternatively, fluorescence lifetime can be detected in the frequency domain with a continuous excitation source and phasor analysis [71-73]. Furthermore, single-photon excitation of fluorescence lifetime and time-gating detection methods have also been adapted for nondestructive imaging in tissue engineering and cell regeneration [26,74-77].

Label-free optical imaging has potential for *in vivo* monitoring of cytotherapies and tissue regeneration after implantation of the biodevices. FLIM performed through a fiber-optic probe was successfully performed to image and characterize the viability of engineered tissue constructs comprised of oral keratinocytes seeded on a collagen scaffold post-implantation in mice [78]. While label-free optical imaging is attractive for *in vivo* monitoring of cytotherapy devices post-implantation, the limited penetration depth of light limits its use to superficial tissues and sites accessible with a fiber-optic probe. Therefore, potential technological enhancements to improve the robustness of label-free nonlinear imaging techniques for clinical applications include the optimization of instrumentation and imaging speed, simplification of data processing, and development of models for data interpretation.

In conclusion, nonlinear optical techniques including SHG imaging and autofluorescence lifetime imaging are impactful tools to image cellular metabolism and the collagen structure. Due to the label-free and non-damaging nature of these imaging modalities, it is possible to assess cells and the ECM in intact tissues over time-course studies of wound healing and tissue regeneration. Additionally, optical imaging can be adapted for in-line monitoring of cellular products for cytotherapies.

Acknowledgements

Figures were created in [Biorender.com](https://biorender.com). Funding sources include NIH NIGMS R35GM142990 and Texas A&M University. We thank Dhavan Sharma and Feng Zhao (Texas A&M University, College Station) for providing aligned and random collagen scaffolds.

Data availability

No data was used for the research described in the article.

References

Papers of particular interest, published within the period of review, have been highlighted as:

* of special interest

1. Aly RM: Current state of stem cell-based therapies: an overview. *Stem Cell Invest* 2020, 7:8.
2. Raffin C, Vo LT, Bluestone JA: Treg cell-based therapies: challenges and perspectives. *Nat Rev Immunol* 2020, 20: 158–172. [PubMed: 31811270]

3. Chavez JC, Bachmeier C, Kharfan-Dabaja MA: CAR T-cell therapy for B-cell lymphomas: clinical trial results of available products. *Ther Adv Hematol* 2019, 10, 2040620719841581. [PubMed: 31019670]
4. Smith BD, Grande DA: The current state of scaffolds for musculoskeletal regenerative applications. *Nat Rev Rheumatol* 2015, 11:213–222. [PubMed: 25776947]
5. Murphy SV, Atala A: 3D bioprinting of tissues and organs. *Nat Biotechnol* 2014, 32:773–785. [PubMed: 25093879]
6. Sharpe ME, Morton D, Rossi A: Nonclinical safety strategies for stem cell therapies. *Toxicol Appl Pharmacol* 2012, 262: 223–231. [PubMed: 22617430]
7. Herberts CA, Kwa MS, Hermesen HP: Risk factors in the development of stem cell therapy. *J Transl Med* 2011, 9:29. [PubMed: 21418664]
8. Odeleye AOO, et al. : Development of an optical system for the non-invasive tracking of stem cell growth on microcarriers. *Biotechnol Bioeng* 2017, 114:2032–2042. [PubMed: 28464210]
9. Suhr H, et al. : In situ microscopy for on-line characterization of cell-populations in bioreactors, including cell-concentration measurements by depth from focus. *Biotechnol Bioeng* 1995, 47:106–116. [PubMed: 18623372]
10. Datta R, et al. : Fluorescence lifetime imaging microscopy: fundamentals and advances in instrumentation, analysis, and applications. *J Biomed Opt* 2020, 25(7), 071203. [PubMed: 32406215]
11. Georgakoudi I, Quinn KP: Optical imaging using endogenous contrast to assess metabolic state. *Annu Rev Biomed Eng* 2012, 14:351–367. [PubMed: 22607264]
12. Kolenc OI, Quinn KP: Evaluating cell metabolism through autofluorescence imaging of NAD(P)H and FAD. *Antioxidants Redox Signal* 2019, 30:875–889.
13. Huang S, Heikal AA, Webb WW: Two-photon fluorescence spectroscopy and microscopy of NAD(P)H and flavoprotein. *Biophys J* 2002, 82:2811–2825. [PubMed: 11964266]
14. Lakowicz JR: Principles of fluorescence spectroscopy. Springer science & business media; 2013.
15. Heaster TM, et al. : Autofluorescence imaging of 3D tumor–macrophage microscale cultures resolves spatial and temporal dynamics of macrophage metabolism. *Cancer Res* 2020, 80:5408–5423. [PubMed: 33093167]
16. Lakowicz JR, et al. : Fluorescence lifetime imaging of free and protein-bound NADH. *Proc Natl Acad Sci U S A* 1992, 89: 1271–1275. [PubMed: 1741380]
17. Nakashima N, et al. : Picosecond fluorescence lifetime of the coenzyme of D-amino acid oxidase. *J Biol Chem* 1980, 255: 5261–5263. [PubMed: 6102996]
18. Walsh AJ, et al. : Classification of T-cell activation via autofluorescence lifetime imaging. *Nat Biomed Eng* 2021, 5:77–88. [PubMed: 32719514]
19. Walsh AJ, et al. : Quantitative optical imaging of primary tumor organoid metabolism predicts drug response in breast cancer. *Cancer Res* 2014, 74:5184–5194. [PubMed: 25100563]
20. Skala MC, et al. : In vivo multiphoton microscopy of NADH and FAD redox states, fluorescence lifetimes, and cellular morphology in precancerous epithelia. *Proc Natl Acad Sci U S A* 2007, 104:19494–19499. [PubMed: 18042710]
21. Theodossiou A, et al. : Autofluorescence imaging to evaluate cellular metabolism. *JoVE* 2021.
22. Dudenkova VV, et al. : Examination of collagen structure and state by the second harmonic generation microscopy. *Biochemistry (Mosc)* 2019, 84:S89–S107. [PubMed: 31213197]
23. Liu Y, et al. : Methods for quantifying fibrillar collagen alignment. *Methods Mol Biol* 2017, 1627:429–451. [PubMed: 28836218]
24. Kirby MA, Heurman AC, Yellon SM: Utility of optical density of picosirius red birefringence for analysis of cross-linked collagen in remodeling of the peripartum cervix for parturition. *Integr Gynecol Obstet J* 2018, 1.
25. Laurence DW, et al. : A pilot study on biaxial mechanical, collagen microstructural, and morphological characterizations of a resected human intracranial aneurysm tissue. *Sci Rep* 2021, 11:3525. [PubMed: 33568740]

26. Shaik TA, et al. : Monitoring changes in biochemical and biomechanical properties of collagenous tissues using label-free and nondestructive optical imaging techniques. *Anal Chem* 2021, 93:3813–3821. [PubMed: 33596051]
27. Hung CW, et al. : Label-free characterization of collagen crosslinking in bone-engineered materials using nonlinear optical microscopy. *Microsc Microanal*; 2021:1–11.
28. Votteler M, et al. : Raman spectroscopy for the non-contact and non-destructive monitoring of collagen damage within tissues. *J Biophot* 2012, 5:47–56.
29. Iannucci LE, et al. : Optical imaging of dynamic collagen processes in health and disease. *Front Mech Eng* 2022, 8.
30. Zhou X, et al. : Light-sheet scattering microscopy to visualize long-term interactions between cells and extracellular matrix. *Front Immunol* 2022, 13, 828634. [PubMed: 35154150]
31. Paganelli A, et al. : Use of confocal microscopy imaging for in vitro assessment of adipose-derived mesenchymal stromal cells seeding on acellular dermal matrices: 3D reconstruction based on collagen autofluorescence. *Skin Res Technol* 2022, 28:133–141. [PubMed: 34555218]
32. Sabo AR, et al. : Label-free imaging of non-deparaffinized sections of the human kidney to determine tissue quality and signatures of disease. *Phys Rep* 2022, 10, e15167.
33. Lakowicz JR: Principles of fluorescence spectroscopy. Vol. MD 21201. Baltimore: Springer US, University of Maryland School of Medicine; 2006.
34. Galvan-Pena S, O'Neill LA: Metabolic reprogramming in macrophage polarization. *Front Immunol* 2014, 5:420. [PubMed: 25228902]
35. Chang CH, et al. : Posttranscriptional control of T cell effector function by aerobic glycolysis. *Cell* 2013, 153:1239–1251. [PubMed: 23746840]
- 36*. Walsh AJ, et al. : Classification of T-cell activation via autofluorescence lifetime imaging. *Nature biomedical engineering* 2021, 5:77–88. This paper found that autofluorescence lifetime imaging of NAD(P)H and FAD combined with machine learning could predict T cell activation state with very high accuracy. These findings suggest that label-free optical methods can be used for non-contact assessment of T cells and quality control of cell based therapies.
37. Wang ZJ, et al. : Classifying T cell activity in autofluorescence intensity images with convolutional neural networks. *J Biophot* 2020, 13, e201960050.
38. Khalil DN, et al. : The new era of cancer immunotherapy: manipulating T-cell activity to overcome malignancy. *Adv Cancer Res* 2015, 128:1–68. [PubMed: 26216629]
39. Long KB and Beatty GL, Harnessing the antitumor potential of macrophages for cancer immunotherapy. (2162-4011 (Print)).
40. Lee C, et al. : Targeting of M2-like tumor-associated macrophages with a melittin-based pro-apoptotic peptide. *Journal for immunotherapy of cancer* 2019, 7:1–14. [PubMed: 30612589]
41. Alfonso-Garcia A, et al. : Label-free identification of macrophage phenotype by fluorescence lifetime imaging microscopy. *J Biomed Opt* 2016, 21(4):46005. [PubMed: 27086689]
42. Heaster TM, et al. : Intravital metabolic autofluorescence imaging captures macrophage heterogeneity across normal and cancerous tissue. *Front Bioeng Biotechnol* 2021, 9:312.
43. Heaster TM, et al. : Autofluorescence imaging of 3D tumor-macrophage microscale cultures resolves spatial and temporal dynamics of macrophage metabolism. *canres*; 2020:2020.0831.
44. Pavillon N, et al. : Noninvasive detection of macrophage activation with single-cell resolution through machine learning. *Proc Natl Acad Sci U S A* 2018, 115:E2676–E2685. [PubMed: 29511099]
45. Miskolci V, et al.: *In vivo* fluorescence lifetime imaging captures metabolic changes in macrophages during wound responses in zebrafish. 2020. 2020.06.16.153361.
46. Suzuki T, et al. : Pulmonary macrophage transplantation therapy. *Nature* 2014, 514:450–454. [PubMed: 25274301]
- 47*. Qian T, et al. : Label-free imaging for quality control of cardiomyocyte differentiation. *Nat Commun* 2021, 12:4580. [PubMed: 34321477] A variety of methods have been established to differentiate human pluripotent stem cells (hPSCs) into cardiomyocytes (CMs). The process is time consuming and there is a need in cardiac medicine to generate functional CMs with high quality in a cost-effective and time-efficient manner. This study has found it possible to predict the differentiation outcome as early as day 1 of the process using optical metabolic imaging

- (OMI). Autofluorescence imaging can resolve metabolic changes between low (< 50%) and high (50%) CM differentiation. This knowledge can potentially be used to optimize the evaluation process and minimize interruption in the differentiation process, allowing high quality cells to be used in drug screening, toxicity testing, disease modeling, and regenerative cell therapy.
48. Yuan Y, et al., Autofluorescence of NADH is a new biomarker for sorting and characterizing cancer stem cells in human glioma. (1757-6512 [Electronic]).
 49. Bonuccelli G, et al., NADH autofluorescence, a new metabolic biomarker for cancer stem cells: identification of Vitamin C and CAPE as natural products targeting "stemness". (1949-2553 [Electronic]).
 50. Gluck MJ, et al. : Detecting structural and inflammatory response after in vivo stretch injury in the rat median nerve via second harmonic generation. *J Neurosci Methods* 2018, 303:68–80. [PubMed: 29454014]
 - 51*. Koudouna E, et al. : Recapitulation of normal collagen architecture in embryonic wounded corneas. *Sci Rep* 2020, 10, 13815. [PubMed: 32796881] The authors revealed the three-dimensional collagen architecture of wounded embryonic corneas during wound healing using second-harmonic generation. They found irregular thin collagen fibers in the early phase of wound healing, and orthogonal arrangement of collagen organization as wound healing progresses. This study reveals that collagen organization in chick embryonic wound healing can recapitulate the native macrostructure of the cornea, suggesting a primer model to understand tissue regeneration.
 52. Kivanany PB, et al. : Assessment of corneal stromal remodeling and regeneration after photorefractive keratectomy. *Sci Rep* 2018, 8, 12580. [PubMed: 30135552]
 53. Israel JS, et al. : Quantification of collagen organization after nerve repair. *Plast Reconstr Surg Glob Open* 2017, 5:e1586. [PubMed: 29632766]
 - 54*. Pichon J, et al. : Label-free 3D characterization of cardiac fibrosis in muscular dystrophy using SHG imaging of cleared tissue. *Biol Cell* 2022, 114:91–103. [PubMed: 34964145] Three-dimensional characterization of cardiac fibrosis network from Duchenne muscular dystrophy rat model by SHG imaging reveals greater deposition, increased density, and profound fiber disorganization of collagen compared with wild-type rats. The study highlights a label-free method for 3D fibrosis network characterization using SHG microscopy and tissue clearing, suggesting a tool to track fibrotic tissue remodeling in disease progression and therapeutic response in clinical.
 55. Fuentes-Corona CG, et al. : Second harmonic generation signal from type I collagen fibers grown in vitro. *Biomed Opt Express* 2019, 10(12):6449–6461. [PubMed: 31853410]
 56. Kabir MM, et al., Application of quantitative second-harmonic generation microscopy to dynamic conditions. (2156-7085 [Print]).
 - 57*. Xydias D, et al., Three-dimensional characterization of collagen remodeling in cell-seeded collagen scaffolds via polarization second harmonic generation. (2156-7085 [Print]). The authors used polarization second harmonic generation (PSHG) to characterize the structure of porous collagen-GAG scaffolds seeded with human umbilical vein endothelial cells and human mesenchymal stem cells over 10 days and found orthogonal net-like architecture development on different days. This study demonstrates the efficacy of PSHG in quantifying the kinetic of cell-induced collagen remodeling over time, which provides novel tools to study cell and microenvironment interactions.
 - 58*. Kourgiantaki A, et al., Neural stem cell delivery via porous collagen scaffolds promotes neuronal differentiation and locomotion recovery in spinal cord injury. (2057-3995 [Electronic]). Engineered porous collagen-based scaffolds can deliver and protect embryonic neural stem cells at spinal cord injury in a mouse model, which enhances neuronal differentiation and locomotion recovery. Their findings imply the potential of improving neural stem cells-based spinal cord injury therapy by grafts of porous collagen-based scaffolds.
 59. VandenHeuvel SN, et al. : Decellularized organ biomatrices facilitate quantifiable in vitro 3D cancer metastasis models. *Soft Matter* 2022, 18:5791–5806. [PubMed: 35894795]
 60. Rezakhaniha R, et al. : Experimental investigation of collagen waviness and orientation in the arterial adventitia using confocal laser scanning microscopy. *Biomech Model Mechanobiol* 2012, 11:461–473. [PubMed: 21744269]

61. Wu S, et al. : Quantitative evaluation of redox ratio and collagen characteristics during breast cancer chemotherapy using two-photon intrinsic imaging. *Biomed Opt Express* 2018, 9(3):1375–1388. [PubMed: 29541528]
62. Syverud BC, Mycek MA, Larkin LM: Quantitative, label-free evaluation of tissue-engineered skeletal muscle through multiphoton microscopy. *Tissue Eng C Methods* 2017, 23(10): 616–626.
63. Lukina MM, et al. : In vivo metabolic and SHG imaging for monitoring of tumor response to chemotherapy. *Cytometry* 2019, 95:47–55. [PubMed: 30329217]
64. Hu L, et al.: Multiphoton microscopy to characterize macrophage function and collagen alignment. *SPIE BiOS*. Vol. PC11965. 2022 [SPIE].
65. Houston JP, Naivar MA, Freyer JP: Digital analysis and sorting of fluorescence lifetime by flow cytometry. *Cytometry* 2010, 77:861–872. [PubMed: 20662090]
66. Cao R, Pankayatselvan V, Houston JP: Cytometric sorting based on the fluorescence lifetime of spectrally overlapping signals. *Opt Express* 2013, 21(12):14816–14831. [PubMed: 23787669]
67. Manna P, Jimenez R: Time and frequency-domain measurement of ground-state recovery times in red fluorescent proteins. *J Phys Chem B* 2015, 119:4944–4954. [PubMed: 25781915]
68. Qi J, et al. : Fast flexible multiphoton fluorescence lifetime imaging using acousto-optic deflector. *Opt Lett* 2013, 38(10): 1697–1699. [PubMed: 23938915]
69. Ahmed-Cox A, et al. : Application of rapid fluorescence lifetime imaging microscopy (RapidFLIM) to examine dynamics of nanoparticle uptake in live cells. *Cells* 2022, 11.
70. Samimi K, et al. : Time-domain single photon-excited autofluorescence lifetime for label-free detection of T cell activation. *Opt Lett* 2021, 46(9):2168–2171. [PubMed: 33929445]
71. Stringari C, et al. : Phasor approach to fluorescence lifetime microscopy distinguishes different metabolic states of germ cells in a live tissue. *Proc Natl Acad Sci U S A* 2011, 108: 13582–13587. [PubMed: 21808026]
72. Ranjit S, et al. : Imaging fibrosis and separating collagens using second harmonic generation and phasor approach to fluorescence lifetime imaging. *Sci Rep* 2015, 5, 13378. [PubMed: 26293987]
73. Sameni S, et al. : The phasor-FLIM fingerprints reveal shifts from OXPHOS to enhanced glycolysis in Huntington Disease. *Sci Rep* 2016, 6, 34755. [PubMed: 27713486]
74. Manning HB, et al. : Detection of cartilage matrix degradation by autofluorescence lifetime. *Matrix Biol* 2013, 32: 32–38. [PubMed: 23266527]
75. Alfonso-Garcia A, et al. : Fiber-based fluorescence lifetime imaging of recellularization processes on vascular tissue constructs. *J Biophot* 2018, 11:e201700391.
76. Li C, et al. : Label-free assessment of collagenase digestion on bovine pericardium properties by fluorescence lifetime imaging. *Ann Biomed Eng* 2018, 46:1870–1881. [PubMed: 30003502]
77. Haudenschild AK, et al. : Non-destructive detection of matrix stabilization correlates with enhanced mechanical properties of self-assembled articular cartilage. *J Tissue Eng Regen Med* 2019, 13:637–648. [PubMed: 30770656]
78. Elahi SF, et al. : Noninvasive optical assessment of implanted engineered tissues correlates with cytokine secretion. *Tissue Eng C Methods* 2018, 24(4):214–221.

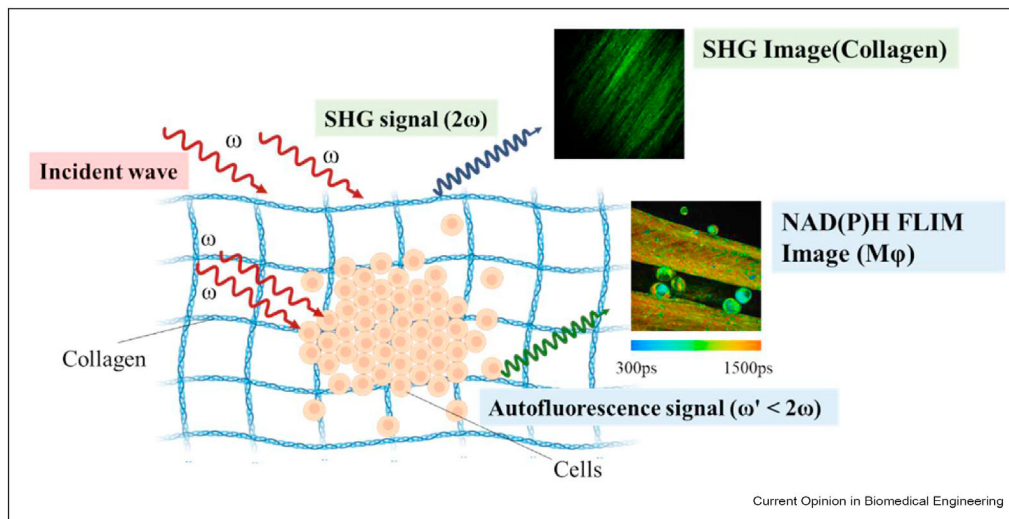
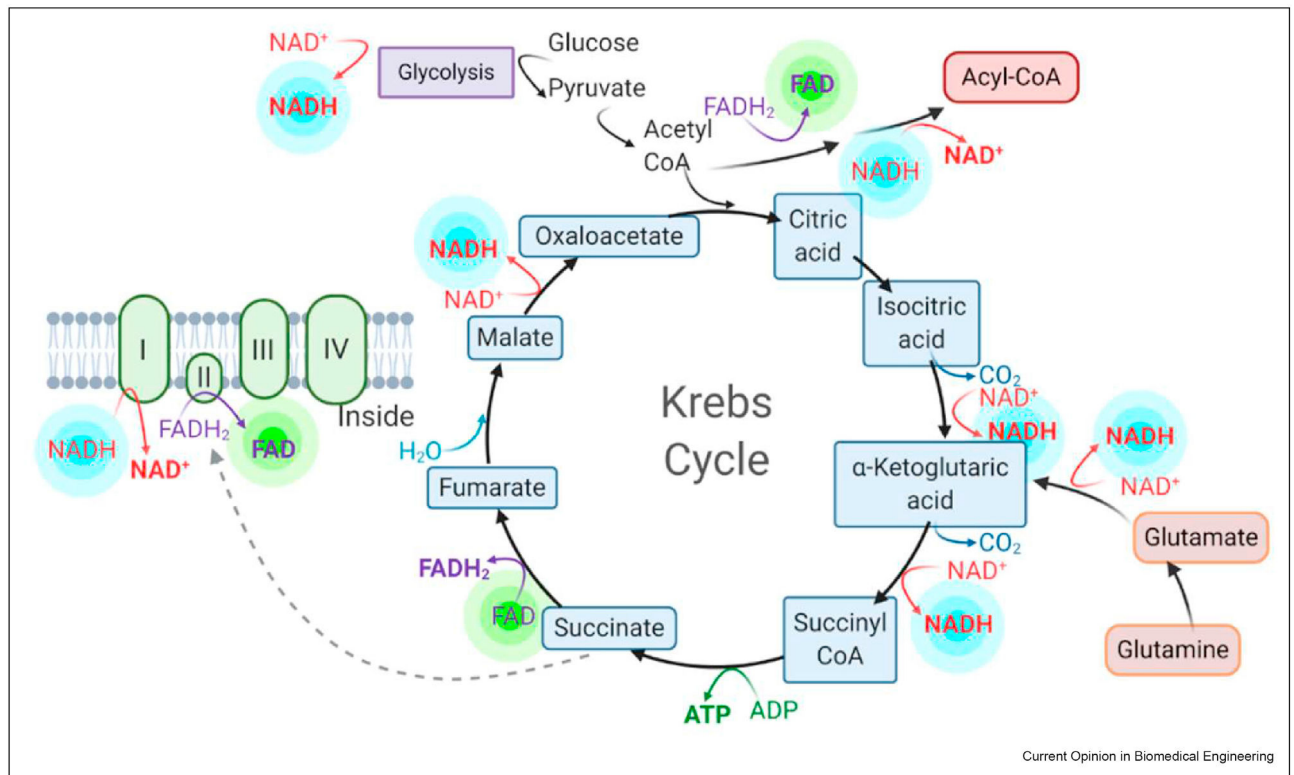


Figure 1.

Optical imaging of cell autofluorescence and collagen second harmonic generation allows label-free and non-contact assessment of cell-based therapies. Second harmonic generation (SHG) occurs when two incident photons with the same frequency (ω) interact with a nonlinear material, such as fibrillar collagen, and generate a new photon with twice the frequency (2ω). Two-photon fluorescence excitation requires simultaneous stimulation of a fluorophore by two photons, and the frequency of the fluorescence emission (ω') is less than twice the excitation frequency (ω). SHG images allow visualization of fibrillar collagen (top insert) and can be used to evaluate the ECM of engineered tissues and scaffolds. Autofluorescence lifetime imaging of NAD(P)H within cells (bottom insert, image of macrophages, $M\phi$, on collagen ECM) provides metabolic information.



Current Opinion in Biomedical Engineering

Figure 2.

NADH and FAD are coenzymes of cellular metabolic reactions. NADH is an electron acceptor in glycolysis and an electron donor in the electron transport chain (ETC), while FAD is the principal electron donor in the ETC. Furthermore, both NADH and FAD are used in other metabolic pathways including the Krebs cycle and glutaminolysis.

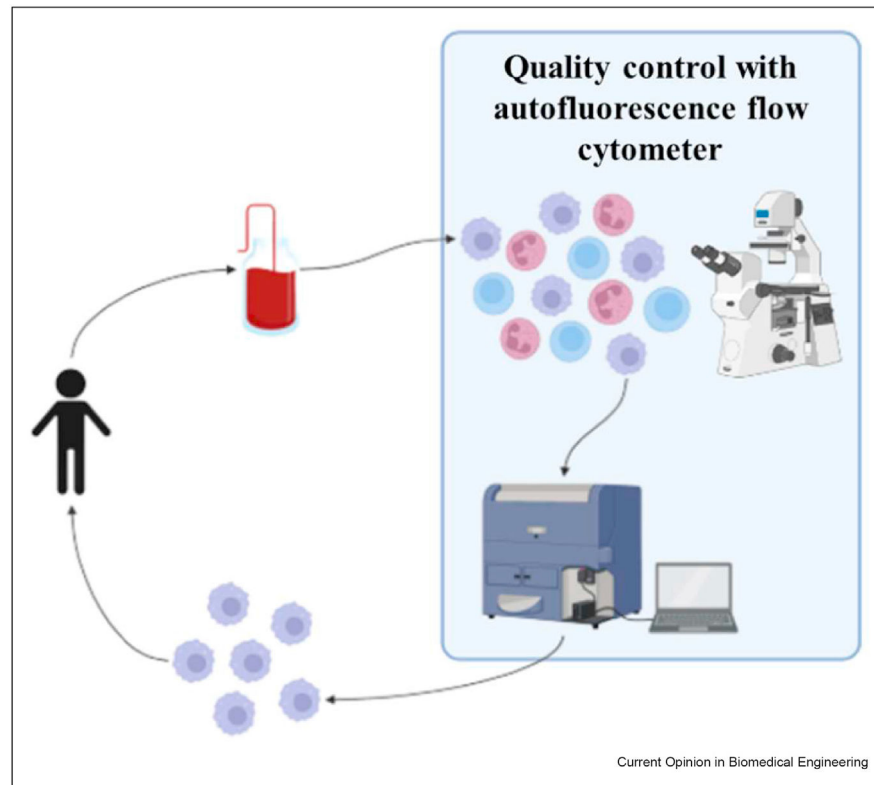


Figure 3. Envisioned process for integration of autofluorescence imaging into the manufacturing process of cytotherapies. In cytotherapies, such as CAR T cell therapies, blood is drawn from the patient and the therapeutic cells are extracted and expanded. For purification or viability assessment, the cells could then be analyzed and sorted using an autofluorescence flow cytometer. Then, the patient is treated with the optimal cells.

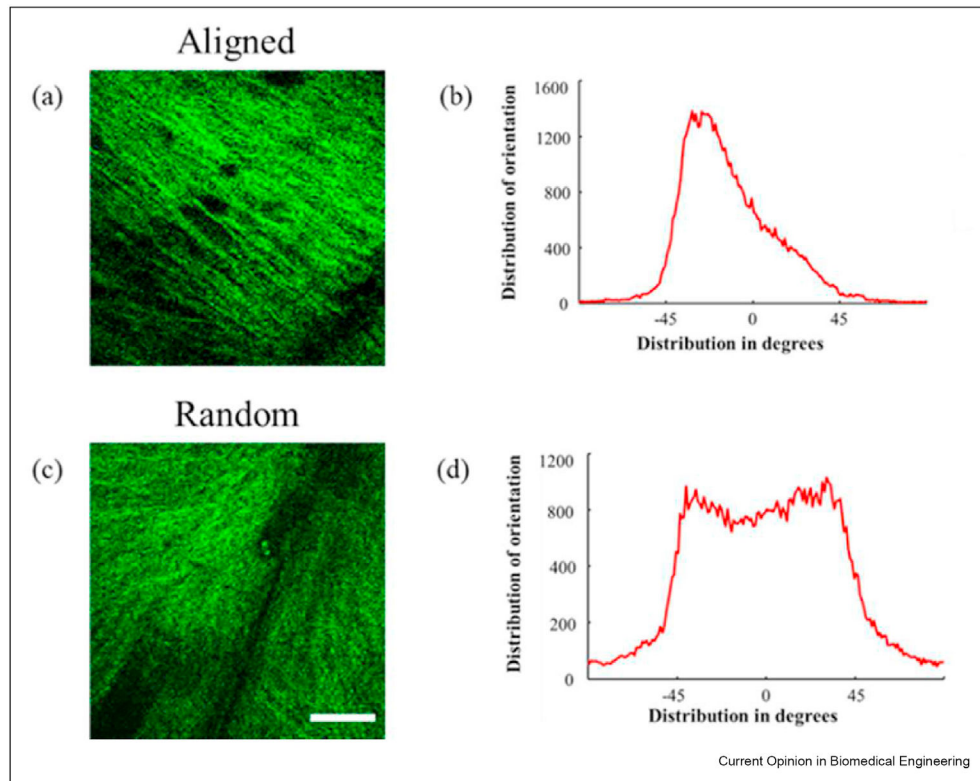


Figure 4. Representative SHG images of human dermal fibroblast sheet-derived extracellular matrix scaffold. (a) Scaffold with aligned fibers and (b) the distribution of fiber orientations within the aligned-fiber scaffold image. (c) Scaffold with random fibers and (d) the distribution of fiber orientations within the random-fiber scaffold image. Fiber orientation was analyzed by the OrientationJ plug in ImageJ [60]. Scale bar = 60 μm .